Study on the molecular mechanisms of wing morphogenesis in *Gryllus bimaculatus*, a model system of hemimetabolous insects

Takahisa Yamashita

Department of Biological Science and Technology
Life and Materials Systems Engineering
Graduate School of Advanced Technology and Science
Tokushima University

September 2023

Contents

ABSTRACT

The acquisition of wings was a key event in insect evolution. As hemimetabolous insects were the first group to acquire functional wings, establishing the mechanisms of wing formation in this group could provide useful insights into their evolution. In this study, we aimed to elucidate the expression and function of the gene *scalloped* (*sd*), which is involved in wing formation in *Drosophila melanogaster*, in *Gryllus bimaculatus* mainly during post-embryonic development. Expression analysis showed that *sd* is expressed in the tergal edge, legs, antennae, labrum, and cerci during embryogenesis and in the distal margin of the wing pads from at least the sixth-instar in the mid to late stages. Because *sd* knockout caused early lethality, nymphal RNA interference experiments were performed. Malformations were observed in the wings, ovipositor, and antennae. By analyzing the effects on wing morphology, it was revealed that *sd* is mainly involved in formation of the margin, possibly through the regulation of cell proliferation. In conclusion, *sd* might regulate the local growth of wing pads and influence wing margin morphology in *Gryllus.*

GENERAL INTRODUCTION

Evolution of insects and wings

Insects are the largest group of animals in the world and have evolved in a diversity proportional to the number of species. Since most insects are winged insects, the acquisition of wings is considered a key factor in the explosive increase of insect species and has been an important model organism in evolutionary development.

Winged insects are classified into two types: holometabolous, which metamorphose from pupa to adult, and hemimetabolous which metamorphose by repeated molting. The process of wing formation differs significantly between holometabolous and hemimetabolous. The holometabolous wing primordium consists of a group of cells called the wing disc, which is one of the imaginal discs.

The wing disc is determined to differentiate into wing cells from embryonic development, and grows separately from other organs. On the other hand, hemimetabolous does not have a wing disc and grows by gradual elongation of the wing primordium (wing pads) on the dorsal plate from the nymphal stage with molting.

History of wing studies

The main themes of study on wings are the search for the origin of ontogeny and the mechanism of formation. There are three different theories of origin: dorsal plate origin, lateral plate origin, and compound origin, and their conclusions have not yet been integrated. In order to examine the organization of origin, it is necessary to study primitive wingless insects and insects with hemimetabolous, which are generally called non-model organisms, making molecular analysis difficult. However, recently, research using hemimetabolous insects has gradually advanced and morphological analyses using

electron microscopy and other techniques have proposed the dual origin theory, which combines dorsal and lateral plates (Mashimo and Machida et al., 2017) and the dorsal origin theory based on homology of gene groups and tissues involved in wing development (Ohde et al., 2017)

In terms of the developmental mechanism of wing disc, it has already been extensively analysed, especially the developmental process from the second instar. In the second instar larvae, the expression of *wingless* (*wg*) defines the wing pouch (wing) and the expression of EGFR defines the notum (body wall) and hinge regions, and both are expressed antagonistically. Subsequently, *apterous* (*ap*) is expressed from the notum to half of the wing pouch, defining the D-V boundary at the wing pouch (Losada et al., 2018) Then in late second instar, the wing master gene *vestigial* (*vg*), induced by *notch* (*N*) expression, is expressed crosswise from the center of the DV boundary.

In the third instar, wing pouch cells are recruited from the center of the *vestigial*-expressed wing pouch and expanded in concentric circles by the FF signal, in which Ds-FT, HIPPO, and *vestigial* signals interact. *vestigial* plays a leading role in this FF signal and has been used as a wing marker gene in various insects for research.

In addition, both Hippo (*hpo*) and Vestigial, which constitute the HIPPO signal, are known to be nuclear translocated and activated by forming a complex with the transcription factor *scalloped* (*sd*). FF signal is expected to elucidate the molecular mechanisms of wing morphological evolution by analyzing changes in the function and expression of its constituent factors in various species.

Transcription factor：*scalloped*

scalloped is a transcription factor belonging to the TEAD family and is widely conserved down to mammals such as mouse.

It is known to be involved in various developmental processes such as organ size regulation, neurogenesis, and wing formation by regulating factors related to cell proliferation and cell cycle such as *CyclinE* and *Diap1*.

In *Drosophila*, *sd* has been reported to be expressed in the eye disc, central nervous system, and peripheral nerves, and in the wing disc, it is expressed throughout the wing pouch, overlapping the *vestigial* region.

Life cycle of the *Gryllus bimaculatus*

Gryllus bimaculatus is an Orthoptera insect. Its life span is approximately one and a half months. Embryonic stage exists from stage one to twenty-four and hatches in approximately eleven to twelve days. The nymphal stage exists first to eighth instar and metamorphoses into an adult after eighth instars. It takes approximately ±1 day of each instar to molt. Regarding the development of wing pads, they are not visible until the fifth instar, and from the sixth instar, protruding tissues are observed at T2 and T3 on the thoracic dorsal plate.

***Gryllus bimaculatus* as a genetic model system**

Gryllus used in this study can be subjected to the RNAi method. RNAi can suppress mRNA expression of target genes by injecting dsRNA with complementary sequences. Currently, parental RNAi and nymphal RNAi methods have been established to study the effects during embryogenesis and larval stages. (Miyawaki et al., 2004; Ronco et al., 2007). In addition, genome editing using the CRISPR/Cas9 system has recently been established. By co-injecting Cas9 and a complementary gRNA sequence to the target, it

is possible to cleave specific sequences. (Knock-out). In *Gryllus*, Knock-out strains have already been established using this technique (Nakamura et al., 2021). In addition, by introducing an exogenous vector into the cleavage site, it is possible to express the exogenous gene followed the target gene expression (knock-in). Using this technique, GFP line has been generated in *Gryllus* by introducing a GFP expression cassette vector into the exon of a target gene（Matsuoka et al., preprinted).

In this study, we developed this knock-in method which is called enhancer trap method. In the enhancer trap method, exogenous genes are introduced into the upstream intron of the target gene, and the expression of the target gene can be tracked by GFP without gene disruption.

INTRODUCTION

Insects comprise the largest group of animals globally, and they have acquired diverse forms in proportion to the number of species. In particular, the group of winged insects known as Pterygota are highly variable, and this group has been widely studied to elucidate the process of wing morphogenesis in insect evolution. *Drosophila melanogaster* is the most extensively studied model system for comprehensively analyzing the molecular mechanisms of wing development (Zecca et al., 2021). In addition, other holometabolous species, such as *Rhopalocera Duméril* and *Tribolium castaneum*, have been also used as model systems in studies of wing evolution (Lai et al., 2018; Nijhout, 1991). However, the use of molecular approaches to investigate wing development in hemimetabolous insects is limited to a few species, such as *Oncopeltus fasciatus* and *Blattella germanica* (Medved et al., 2015; Fernandez-Nicolas et al., 2022), and the mechanisms remain largely unknown.

The processes of wing development fundamentally differ between holometabolous and hemimetabolous insects. Holometabolous insects drastically change their morphology at the larval stage through metamorphosis, with adult organs such as wings being formed from imaginal discs. By contrast, in hemimetabolous insects, wings develop from primordia (wing pads), not imaginal discs, as miniature adult wings. Thus, to advance our current understanding of the evolution of wings in insects, the molecular mechanisms of wing development in hemimetabolous insects should be investigated and compared with those of holometabolous insects.

In the present study, we used *Gryllus bimaculatus* as a model system to investigate the mechanisms of wing development in hemimetabolous insects. This species has been used as a genetic model system in various biological fields, allowing the application of

RNA interference (RNAi) methods and genome editing with clustered regularly interspaced short palindromic repeats (CRISPR)/CRISPR-associated protein 9 (Cas9), (Horch, 2017; Mito and Noji, 2008). Ohde, Mito, & Niimi (2022) showed that the wing pads in *Gryllus* grow through expansion of the lateral targa. Furthermore, they found that *vestigial*-dependent lateral tergum formation and growth signals transmitted via the Wnt, Fat/Dachsous, and Hippo pathways might be important in this process (Ohde et al., 2022).

In this study, we aimed to elucidate the expression and function of the gene *scalloped* (*sd*) in *Gryllus* mainly during post-embryonic development (nymphal stages). This gene encodes a transcription factor belonging to the TEA/ATTS domain (TEAD) family. Previously, *sd* was shown to act as a downstream effector in the Wnt and Hippo pathways and participate in nervous system development and wing formation by forming a complex with either Vestigal (Vg) or Yorkie (Yki) for nuclear translocation and cell growth regulation in *Drosophila* (Goulev et al., 2008; Simmonds et al., 1998; Halder & Carroll, 2022). Specifically, we conducted functional and expression analysis using nymphal RNAi, *in situ* hybridization, and enhancer trap lines.

RESULTS

Gene and amino acid structures of *sd* in *Gryllus bimaculatus*

Using a previously reported partial cDNA sequence of *Gryllus sd* (Bando et al., 2009) and the transcriptomic data of early-to-midstage *Gryllus* embryos (Mito et al., unpublished data), we determined the full-length coding sequence of *Gryllus sd*. The cDNA sequence was deposited into GenBank (Accession No: OQ885480). Its translated amino acid sequence showed high homology (99% and 74%, respectively) with the functional domains of *Drosophila* sd protein, namely TEAD and YAP-binding domain (YBD), as presented in Figure 1a. The *sd* cDNA sequence was mapped onto the *Gryllus bimaculatus* genome sequence as 11 exons (Ylla et al., 2021; Figure 1b). *Gryllus sd* (approximately 295 kb) was 12.6-fold longer than *Drosophila sd* (approximately 23 kb). The presence of a giant intron between the first and second exons represented a common feature in *Gryllus* and *Drosophila sd* (Campbell et al., 1992; Figure 1b).

Expression patterns of *Gryllus sd* during embryogenesis

To examine the expression patterns of *sd* during *Gryllus* embryogenesis, we performed *in situ* hybridization. *sd* was expressed in a striped pattern in antennae and all T1–T3 legs and in a spotted pattern in the cerci of embryos in stage 10 and subsequent stages (staging based on Donoughe & Extavour, 2016; Figure 2a–g). Expression was also observed in the dorsal segments in stage 16 (Figure 2d, h). For the negative control, sense expression was compared to *sd* expression in stages 10, 12, and 16 (Figure 3a-f).

Because of a technical problem caused by a thickened cuticle, whole-mount *in situ* hybridization could only be performed with clear staining up to stage 16. To analyze expression after this stage, we generated an *sd*-eGFP enhancer trap line by knocking-in

the eGFP expression vector upstream of the *sd* locus (Figure 4a-d). eGFP expression patterns in the embryos of the *sd* enhancer trap line were compared to the *sd* expression patterns obtained by *in situ* hybridization. The comparison indicated that eGFP expression fundamentally corresponded to *sd* expression (Figure 2a′–h′ compared to Figure 2a–h), validating the entrapment of native *sd* enhancers. In stage 22, the expression pattern featured more fine spots in the dorsal segments, legs, and cerci and more fine stripes in antennae (Figure 2i–o). The spot expression corresponded to the position of bristles (data not shown; see Figure 10a-j for expression in wing bristles).

Expression dynamics of *Gryllus sd* in wing pads during final-instar development

To examine *sd* expression in wing pads (Henceforth, unless specified otherwise, wing pads refer to forewings), we first observed the sixth-instar nymphs of the *sd* enhancer trap line, at which stage wing pads are visible. We observed faint *sd* expression in the distal margin area (Figure 5a-e). However, it was technically difficult to observe the continuous expression dynamics in sixth-instar wing pads. Therefore, we observed wing pads every 24 h in final-instar (eighth-instar) nymphs. The eighth instar occurred on days 8–9. We defined days 1–3 as the early stage, days 4–6 as the midstage, and days 7–8 as the late stage. Because eighth-instar wing pad tissue is encased in the cuticle, either the dorsal or ventral side cuticle was removed for observation (Figure 6a–e, j–n, a′-e′, j′–n′ and Figure 7a-d). During the early stage, extremely weak *sd* expression was observed on the distal side of wing pads (Figure 6a′–c′, j′–l′). During the midstage, expression was clearly observed at the distal margin and central trachea of wing pads (Figure 6d′-f′, m′–p′). From the late-mid to early-late stage, *sd* expression increased in the margin, and additional expression appeared on the anterior side of the proximal margin and in the bristle-

concentrated region on the posterior side (Figure 6d′–g′, m′–p′). The additional expression domains corresponded to staining in the wing pad by *in situ* hybridization (Figure 8a-m). *sd*-expressing cells in the bristle-concentrated region on the posterior side were positively stained by anti-HRP antibody; thus, *sd*-expressing cells are likely neuronal cells.

On day 8, the expression of *sd* in wing pads appeared to decline. However, this phenomenon might have been observed because the thickened adult cuticle prevented the detection of eGFP fluorescence. In the adult wing, *sd* expression domains were maintained at lower levels. Conversely, the relative expression might be underestimated because the wing was too thin to be removed for eGFP observation.

Although no clear differences were observed between males and females, the female expression area in the margin on days 6–7 appeared to be slightly wider than that of males (Figure 6f′, g′, o′, p′). We further observed the hindwing on day 6 in the eighth instar, and expression was also observed in the distal and proximal areas and in several veins. However, distal expression of the hindwing was more restricted to the margin than to the forewing (Figure 9a-e).

Effect of *Gryllus sd* KO during embryogenesis

Previous expression analysis suggested that *sd* is involved in wing development. Therefore, we performed gene KO experiments to investigate the effect of loss of function of *sd* in *Gryllus.* gRNAs were designed within the coding region corresponding to TEAD and microinjected with Cas9 proteins into early-stage embryos (Figure 11a). In the injected generation (G0), 87% of individuals turned black and died in embryonic stages 12–15, whereas 11% partially turned black and died in later stages (stages 15–24). The embryos that died in later stages showed eye defects and shortened antennae (Figure 11b–

i). In addition, 2% of injected individuals hatched. In 2 of 10 hatched individuals, the distal part of the legs did not form normally, and the antennae and eyes had defects (Figure 11j–m), while 8 of 10 hatched individuals appeared to have normal morphology. The affected nymphs appeared to be missing the tergal edge. However, it was not possible to continue observations of the effect on tergal edge formation because they died within one day of hatching. These hatched individuals seem to be weakly or not affected by CRISPR/Cas9 mutagenesis, possibly because the induced mutation was in-frame or only because a small number of cells were mutated.

To further validate the *sd* KO phenotypes, we performed RNAi in parental individuals (parental RNAi; Ronco et al., 2007). All RNAi-treated individuals turned black and died in embryonic stages 12–15, as observed in the KO experiments (data not shown). Thus, *Gryllus sd* is essential for proper morphogenesis of the legs, antennae, and eyes during embryogenesis.

Effect of nymphal RNAi for *Gryllus sd* on external organ formation

Because we were unable to generate a *sd* KO line because of lethality, we performed nymphal RNAi to evaluate the effect of *sd* knockdown on wing development during the nymphal stages. In brief, 3 μg of dsRNA were injected into third- and seventh-instar nymphs (Figure 12a-c). We detected morphological defects in wings, antennae, legs, ovipositors, and cerci in RNAi-treated adult crickets (Figure 13a-g). In both female and male crickets, similar defects were also detected in these tissues, excluding ovipositors. In adults injected with dsRNA in the seventh instar, the ovipositors and cerci were curved,

and antennae were bent or missing (Figure 13d, e). Wings and legs were partially malformed, and residues of nymphal cuticle frequently remained attached. In adults injected with dsRNA in the third instar, cerci and antennae formed normally, but ovipositors were shortened. Some legs were missing, and wings were largely defected (Figure 13f, g).

Effects of *Gryllus sd* RNAi on wing morphogenesis

Because injecting 3 μg of dsRNA into third-instar nymphs led to severe wing defects, it was difficult to examine the effect on wing morphology (Figure 14a–d). Therefore, we performed additional RNAi experiments by injecting a smaller amount (0.03 μg) of dsRNA into third- and seventh-instar nymphs. We obtained adult crickets with a more moderate wing phenotype compared to the effect of injecting 3 μg of dsRNA (Figure 14e–i). In moderately affected crickets, smaller wings were formed (Figure 14e–i). Adults in which dsRNA was injected in the third instar had smaller wings than those injected with dsRNA in the seventh instar. In addition, injecting 3 μg of dsRNA in the seventh instar did not lead to severe phenotypes (data not shown). Comparison of the merge illustration revealed a large defect on the distal side as well as a defect on the proximal margins (Figure 14h, i). No significant difference was observed between males and females (Figure 14e–i for females, Figure 15a-e for males).

To specify the defected area of the wing, we performed landmark analysis in affected male wings (Figures 14j and 15a-e). The area of the distal margin of affected wings was reduced to 53% of that of wild-type wings. The dorsal–ventral length, mirror, and chord areas also reduced to 75%, 65%, and 78%, of the wild-type values, respectively, whereas the harp and anterior–posterior length were not significantly affected. In terms of the

overall area, wings were 22% smaller than the wild-type wings (Figures 14j and 16). Because *sd* regulates cell proliferation in *Drosophila*, we performed the EdU assay on eighth-instar wing pads, and the numbers of proliferating cells in the margin area were reduced by 78% and 84% on days 1 and 3, respectively (Figures 14k and 17a-d). Of note, the total number of cells in this area was also reduced by 30% and 20% on days 1 and 3, respectively (Figure 14k). Thus, *sd* knockdown severely affected the formation of the distal area of the wing, leading to decreased cell proliferation.

DISCUSSION

This study investigated the role of *sd* in wing development in *Gryllus bimaculatus*. Functional analyses using RNAi experiments showed that *Gryllus sd* is involved in the morphogenesis of the wing margin. The injection of high concentrations of dsRNA into third-instar nymphs resulted in significant wing defects, whereas the injection of low dsRNA concentrations or injection into seventh-instar nymphs resulted in defects of the outer margin.

In the RNAi experiments, the injection of high concentrations of dsRNA into third-instar nymphs resulted in severe wing defects, whereas the injection of low concentrations of dsRNA into third-instar nymphs or low or high concentrations into seventh-instar nymphs resulted in defects in the distal area.

In the low-concentration dsRNA experiment, both treatment in the third and seventh instars resulted in defects in the distal area, with the earlier introduction resulting in larger defects. This suggests that the control of morphogenesis by *sd* in the distal margin is continuous during the nymphal stages. In addition, the introduction of high concentrations of dsRNA in the third instar did not result in proper growth of the wing

primordium, and almost no adult wings were formed. Conversely, with the injection of low concentrations of dsRNA, the wing primordium grew sufficiently; however, the distal area of the adult wing was defective.

A possible reason for the large wing defects caused by the injection of high concentrations of dsRNA in the third instar is that *sd* functions in two stages; namely, it promotes primordium growth in the early stages and elongation of the distal side of the primordium in the late stages when it has grown sufficiently and patterning has been determined. Treatment with high concentrations of dsRNA in seventh-instar nymphs, which only resulted in defects in the distal area in the adult wing, also supports this view.

Inhibition of primordium growth in early-stage nymphs might result in the loss of wing-forming area, which could inhibit the formation of the wing itself. Additionally, because of the small size of the primordium in early-stage nymphs, the threshold for the amount of *sd* required for proper growth might be lower than that required for distal elongation in late-stage nymphs**.** In addition, the EdU experiment showed that fewer proliferating cells were present in the margin area of RNAi-treated individuals; thus, *sd* is likely involved in growth through controlling cell proliferation. *sd* is considered to control cell proliferation by regulating *cyclin E* in *Drosophila milanogaster*, indicating that *sd* function is conserved across species (Goulev et al., 2008; Wu et al., 2008; Zhang et al., 2008). Both the severe and moderate phenotypes obtained in these experiments might be attributable to inhibition of the growth of wing pad margins in a continuous manner in all instars.

The function of *sd* in the *Drosophila* wing has been extensively investigated. For instance, notching and significant wing loss have been reported as phenotypes in

Drosophila sd mutants (Delanoue et al., 2004; Goulev et al., 2008; Srivastava et al., 2002). Moderate and severe phenotypes were also observed in crickets. However, morphometric analysis of *Gryllus* wings showed that the length of the anterior–posterior axis in RNAi-treated individuals was almost unchanged compared to the wild-type length (0.95-fold), with only the proximal–distal axis direction changing. By contrast, notching of both the anterior–posterior and proximal–distal axes was reported in *Drosophila*. These differences could be correlated to differences in the expression pattern of *sd*. Expression pattern analysis of *Gryllus* wing pads showed that *sd* was expressed in the outer margin. *sd* expression was also observed in sixth-instar wing pads. Meanwhile, *sd* is expressed in the entire wing pouch of third-instar *Drosophila* larvae (Campbell et al., 1992; Guss et al., 2013; Ruiz-Losada et al., 2018; Figure 18). *Sd*-mediated growth signals extend outward from the *vg* boundary enhancer activity, which crosses the center of the wing pouch, with differences resulting in different phenotypes (Zecca et al., 2007, 2010). Ohde et al (2022) reported that factors involved in *Drosophila* wing growth signaling are conserved in the margin tissue of early *Gryllus* nymphs. The expression pattern of *sd* and its regulation of margin growth are consistent with previous reports. Although *sd* and *vg* form a complex and function together, being expressed in basically the same regions, the phenotypes observed following *sd* KO and RNAi, such as defects in antennae, eyes, legs, and ovipositors, have not been reported for *vg*. This might be attributable to the repression of functions related to the Hippo pathway when *vg* is complexed with *yki*. In *Drosophila*, the Hippo pathway is known to be involved in the development of the nervous system throughout the body, and the results correlate with expression patterns and phenotypes.

Regarding the expression peak, *Gryllus sd* was barely expressed in the early stage, and a peak was observed at the mid-to-late stages in the eighth instar. This result contrasted with the findings for *Drosophila sd*, which is expressed ubiquitously in third-instar larvae. This difference might correspond to differences in the mode of development between *Drosophila* and *Gryllus*. *Gryllus* has a longer nymph period than *Drosophila* with stepwise wing pad development. By contrast, *Drosophila* has a short period of rapid wing formation from the imaginal disc. Changes in the areas and timing of *sd* expression might correspond to changes in the developmental mode of wings.

In conclusion, this study revealed that *Gryllus sd* is involved in the formation of antennae, ovipositors, cerci, legs, and wings. In particular, *Gryllus* showed timing and region-specific expression in different stages. This expression was correlated with the disproportionate timing of wing pad growth during the long nymphal period. *sd* expression is involved in the morphogenesis of the margin area, and it helps to characterize the elongation of *Gryllus* wings in a proximal–distal direction. *sd* function is conserved in *Gryllus* and *Drosophila*, and some morphological evolution of the wing might be attributable to upstream factors regulating *sd* expression or *cis* regulation, potentially driving the change in *sd* expression.

FUTURE WORKS

It is necessary to overcome the problems of enhancer traps to develop the experimental system further in the future. Although the enhancer trap reflects the expression of the target gene, it does not directly indicate the localization of the target protein. Therefore, it needs to be validated by comparison with the expression of endogenous mRNA. In addition, this method cannot determine the nuclear translocation

behavior of transcription factors such as *sd*, which is the target gene of this study, and thus cannot be used to determine the exact timing of activation. These problems could be solved by fusing eGFP with the target protein. By using a fusion protein strain, the behavior of the target protein can be observed directly, allowing confirmation of the protein's localization. The expression of fusion proteins requires the establishment of MMEJ and SSODN methods, which insert exogenous genes into the target sequence precisely in single nucleotide level.In the future, these methods will be used to generate reporter strains of various wing-related genes, and cross them to observe the interaction of multiple genes.

In studying the mechanisms of wing formation, it is particularly important to investigate the behavior of HIPPO signals and *vestigial* genes associated with *sd* at the same time, and the expression patterns of morphogens such as *wingless* are also very important. These analyses are expected to provide the first comprehensive details of wing formation mechanisms in hemimetabolous insects in the future.

MATERIALS AND METHODS

Animals

Adults and nymphs of the *Gryllus bimaculatus* white-eyed mutant strain (Mito and Noji, 2008; Ylla et al., 2021) were reared under a 5-h/19-h light/dark cycle at 30°C and 30% relative humidity. Fertilized eggs were collected on wet kitchen towels and incubated at 30°C in a plastic dish.

Cloning

To clone *Gryllus sd* cDNA and use it as template to synthesize double-stranded RNAs (dsRNAs) and RNA probes, total RNA was extracted from adult cricket legs using Isogen (Nippon-Gene, Tokyo, Japan), and RT-PCR was performed using the Superscript First-Strand Synthesis Kit (Invitrogen, Waltham, MA, USA) with Oligo dT primer. The full-length of the coding sequence of *Gryllus sd* cDNA was cloned by PCR using primers designed using the obtained *Gryllus* cDNA sequence data (Primer-3 and Primer-4; Table 1).

In situ hybridization of embryos

Embryos were fixed with 4% paraformaldehyde (PFA) in phosphate-buffered saline with 0.1% Tween 20 (PBST) for 12 h at 4°C in a refrigerator. *In situ* hybridization was performed as previously described (Zhang et al., 2005). The template DNAs for RNA probes were prepared by PCR amplification using the cloned *sd* cDNA as a template and primers carrying the T7 promoter sequence (Primer-13 and Primer-16; Table 1).

Digoxigenin-labeled antisense RNA probes were synthesized using T7 RNA Polymerase (Invitrogen).

Preparation of wing pads

Eighth-instar wing pads were cut with dissecting scissors, and then the dorsal or ventral side of the cuticle was removed from the internal cell layer. The cell layer-attached side of the cuticle was used to measure eGFP fluorescence in the enhancer trap line (see Figure 7).

***In situ* hybridization of wing pads**

Wing pads were fixed with 4% PFA in PBST for 20 min at room temperature. The conditions of *in situ* hybridization were modified from those for embryos described by (Zhang et al., 2005). In the modified procedure, proteinase K was diluted to 1/250 (2-fold in the case of embryos), and the hybridization temperature was at 60°C (70°C for embryos). The template DNAs for RNA probes were prepared by PCR amplification using the cloned *sd* cDNA as a template with Primer-9 and Primer-16 (Table 1).

Immunocytochemistry of wing pads

Wing pads were fixed with 4% PFA in PBST for 30 min at 20°C. After fixation, wing pads were washed in PBST and blocked with 4% blocking reagent (Roche, Basel, Switzerland) in PBST. These procedures were followed by incubation with anti-HRP antibody diluted 1:200 in PBST for 3 h at room temperature. To counterstain nuclei, wing pads were incubated with DAPI diluted 1:1000 in PBST for 15 min at room temperature

after immunostaining. A confocal laser-scanning microscope (TCS SP5, Leica, Wetzlar, Germany) was used for fluorescence observation.

Design of the guide RNAs (gRNAs)

gRNAs were designed using CasOT (Xiao et al., 2014) or CRISPR direct (Naito et al., 2015). For the gene knock-in experiment, three target sites were selected from 2 kb upstream to the first nucleotide of the coding region to 1 kb downstream of this region (gRNA-1, gRNA-2, and gRNA-3; Figure 4, Table 1). For the gene knockout (KO) experiment, two target sites were selected within TEAD (gRNA-4 and gRNA-5; see Figure 4, Table 1).

Knock-in (KI) and KO experiments using the CRISPR/Cas9 system

For the enhancer trap experiment, the eGFP expression vector DsRed bait-G′act-eGFP was used as a KI donor vector (Matsuoka et al., 2021). The injection solution contained the donor vector, Cas9 protein (TAKARA, Kusatsu, Japan), gRNA for *sd*, and gRNA for the donor vector at final concentrations of 100, 100, 50, and 50 ng/µl, respectively. Injection for the KI experiment was performed using a microinjector (Nanoject II, Dramond Scientific), and 2.3 nl of the injection solution were injected into an egg at 2–3 h after egg laying. Genotyping PCR was performed to detect genome-integrated donor vectors using G1 eGFP-positive embryo genomes. Primers were designed to amplify the sequence including the junction site between an integrated eGFP vector and *sd* (Primer-1 and Primer-2; Figure 2, Table 1).

For the *sd* KO experiment, the injection solution contained Cas9 protein (TAKARA) and gRNAs (gRNA-4 and gRNA-5) at final concentrations of 100 and 50 ng/μl, respectively. The injection was performed as described previously.

dsRNA synthesis and RNAi

The template DNA of dsRNAs was synthesized by PCR using the cloned *sd* cDNA. The used primers were designed by adding the T7 promoter sequence to *sd*-specific sequences (Primer-5, Primer-6, Primer-7, Primer-8; Table 1). The two non-overlapping dsRNAs for *sd* of 198 (dsRNA-1) and 450 bp (dsRNA-2) in length were used for the RNAi experiments using the MEGAScript T7 Kit (Invitrogen). The final concentration of dsRNA was adjusted to 0.2 or 20 μM, and dsRNA was injected to the fourth abdominal segment of each nymph. Then, 560 nl of dsRNA were injected into each nymph using a microinjector (Nanoject II).

qPCR

To prepare *Gryllus* cDNA as the qPCR template, total RNA was extracted from the T2 and T3 segments with the legs removed. cDNA was synthesized using the Superscript First-Strand Synthesis Kit. Power SYBR Green PCR Master Mix (Applied Biosystems, Waltham, MA, USA) was used for qPCR on an ABI 7900 Real-Time PCR System (Applied Biosystems) under the following conditions: 95°C for 10 min followed by 40 cycles of 95°C for 15 s, 60°C for 30 s, and 72°C for 30 s with a concentration of 0.4 μM for each primer. Relative expression was determined using the delta–delta Ct method. *β-actin* was used as a reference gene. All reactions were performed in triplicate as technical

replicates. The primers used in our qPCR are listed in Table 1. Student's *t*-test was used to verify significant differences ($p < 0.05$).

Measurement of wing sizes

The nomenclature of the subdivided areas of a male wing excluding the distal "margin" follows Montealegre-Z, Jonsson, & Robert (2009; see Figure 15). Landmarks based on Klingenberg, Debat, & Roff. (2010) were defined to measure the areas in wings of wild-type and *sd* RNAi crickets (see Figure 15). In addition, two lines (Lines 1 and 2) were defined to measure the size of wings in the anterior–posterior and proximal–distal directions. Line 1 was defined as the vertical line from the edge of plectrum to the anterior edge of the wing. Line 2 was defined as the line from the proximal end of the cubital vein to the most distal point of the wing along the proximal–distal axis. The lengths and areas were measured using Image-J (Rasband, 1997-2012; http://imagej.nih.gov/ij/). Student's *t*-test was used to verify significant differences ($p < 0.05$).

Cell proliferation assay

The cell proliferation assay was performed using the Click-iT EdU Alexa Fluor 488 Imaging Kit (Invitrogen). 5-Ethynyl-2′-deoxyuridine (EdU) was injected to the fourth abdominal segments of eighth-instar nymphs. After 24 h, wing pads were dissected and fixed in 4% PFA in PBST for 30 min. EdU-incorporating cells were detected according to the manufacturer's instructions. A confocal laser-scanning microscope (TCS SP5) was used for fluorescence observation. Student's *t*-test was used to verify significant differences ($p < 0.05$).

ACKNOWLEDGEMENT

I appreciate Professor Taro Mito for his many years of guidance in the completion of this experiment. I also appreciate Assistant Professor Yoshiyasu Ishimaru, Dr. Sayuri Tomonari (technical staff), Assistant Professor Takahito Watanabe, and Ms. Kayoko Tada for their many advice and helping in the experiments and thesis writing.

I would also like to thank Shogo Tanabe, Masamitsu Takai, Mayuko Matsuda, Natsuki Uemura, and Tommy who welcomed me to this laboratory and gave me a special home. You are the very reason why I have been doing this research. I just want to say thank you. I will cherish all memories with you.

REFERENCES

Bando, T., Mito, T., Maeda, Y., Nakamura, T., Ito, F., Watanabe, T., Ohuchi, H., & Noji, S. (2009). Regulation of leg size and shape by the dachsous/fat signalling pathway during regeneration. Development, 136, 2235–2245. doi: 10.1242/dev.035204.

Campbell, S., Inamdar, M., Rodrigues, V., Raghavan, V., Palazzolo, M., & Chovnick, A. (1992). The scalloped gene encodes a novel, evolutionarily conserved transcription factor required for sensory organ differentiation in drosophila. Genes & Development, 6, 367–379. doi: 10.1101/gad.6.3.367.

Delanoue, R., Legent, K., Godefroy, N., Flagiello, D., Dutriaux, A., Vaudin, P., Becker, J. L., & Silber, J. (2004). The drosophila wing differentiation factor vestigial–scalloped is required for cell proliferation and cell survival at the dorso-ventral boundary of the wing imaginal disc. Cell Death & Differentiation, 11, 110–122. doi: 10.1038/sj.cdd.4401321.

Donoughe, S., & Extavour, C. G. (2016). Embryonic development of the cricket Gryllus bimaculatus. Developmental Biology, 411, 140–156. doi: 10.1016/j.ydbio.2015.04.009.

Fernandez-Nicolas, A., Ventos-Alfonso, A., Kamsoi, O., Clark-Hachtel, C., Tomoyasu, Y., & Belles, X. (2022). Broad complex and wing development in cockroaches. Insect Biochemistry & Molecular Biology, 147, 103798. doi: 10.1016/j.ibmb.2022.103798.

Goulev, Y., Fauny, J. D., Gonzalez-Marti, B., Flagiello, D., Silber, J., & Zider, A. (2008). Scalloped interacts with Yorkie, the nuclear effector of the hippo tumor-

suppressor pathway in drosophila. Current Biology, 18, 435–441. doi: 10.1016/j.cub.2008.02.034.

Guss, K. A., Benson, M., Gubitosi, N., Brondell, K., Broadie, K., & Skeath, J. B. (2013). Expression and function of scalloped during drosophila development. Developmental Dynamics, 242, 874–885. doi: 10.1002/dvdy.23942.

Halder, G., & Carroll, S. B. (2001). Binding of the vestigial co-factor switches the DNA-target selectivity of the scalloped selector protein. Development, 128, 3295–3305. doi: 10.1242/dev.128.17.3295

Klingenberg, C. P., Debat, V., & Roff, D. A. (2010). Quantitative genetics of shape in cricket wings: Developmental integration in a functional structure. Evolution, 64, 2935–2951. doi: 10.1111/j.1558-5646.2010.01030.x.

Lai, Y. T., Deem, K. D., Borràs-Castells, F., Sambrani, N., Rudolf, H., Suryamohan, K., El-Sherif, E., … Tomoyasu, Y. (2018). Enhancer identification and activity evaluation in the red flour beetle, Tribolium castaneum. Development, 145, 160663. doi: 10.1242/dev.160663.Matsuoka, Y., Nakamura, T., Watanabe, T., Barnett, A. A., Noji, S., Mito, T., & Extavour, C. G. (2021). Establishment of CRISPR/Cas9-based knock-in in a hemimetabolous insect: Targeted gene tagging in the cricket Gryllus bimaculatus. bioRxiv. doi: 10.1101/2021.05.10.441399.

Matsuoka, Y., Nakamura, T., Watanabe, T., Barnett, A. A., Noji, S., Mito, T., & Extavour, C. G. (2021). Establishment of CRISPR/Cas9-based knock-in in a hemimetabolous insect: targeted gene tagging in the cricket Gryllus bimaculatus. BioRxiv, doi.org/10.1101/2021.05.10.441399.

Mito, T., & Noji, S. (2008). The two-spotted cricket *Gryllus bimaculatus*: An emerging model for developmental and regeneration studies. Cold Spring Harbor Protocols, 2008, pdb.emo110. doi: 10.1101/pdb.emo110.

Montealegre-Z, F., Jonsson, T., & Robert, D. (2011). Sound radiation and wing mechanics in stridulating field crickets (Orthoptera: Gryllidae). Journal of Experimental Biology, 214, 2105–2117. doi: 10.1242/jeb.056283.

Naito, Y., Hino, K., Bono, H., & Ui-Tei, K. (2015). CRISPRdirect: Software for designing CRISPR/Cas guide RNA with reduced off-target sites. Bioinformatics, 31, 1120–1123. doi: 10.1093/bioinformatics/btu743.

Nijhout, H. F. (1991). The development and evolution of butterfly wing patterns. Smithsonian Institution Press, 1991, doi.org/10.1093/aesa/85.6.808.

Ohde, T., Mito, T., & Niimi, T. (2022). A hemimetabolous wing development suggests the wing origin from lateral tergum of a wingless ancestor. Nature Communications, 13, 979. doi: 10.1038/s41467-022-28624-x.

Rasband, W. S. (1997-2012). ImageJ. National Institutes of Health, Bethesda, Maryland, USA. http://imagej.nih.gov/ij/.

Ronco, M., Uda, T., Mito, T., Minelli, A., Noji, S., & Klingler, M. (2007). Antenna and all gnathal appendages are similarly transformed by homothorax knock-down in the cricket Gryllus bimaculatus. Developmental Biology, 313, 80–92. 10.1016/j.ydbio.2007.09.059.

Ruiz-Losada, M., Blom-Dahl, D., Córdoba, S., & Estella, C. (2018). Specification and patterning of drosophila appendages. Journal of Developmental Biology, 6, 17. doi: 10.3390/jdb6030017.

Simmonds, A. J., Liu, X., Soanes, K. H., Krause, H. M., Irvine, K. D., & Bell, J. B. (1998).

Molecular interactions between vestigial and scalloped promote wing formation in drosophila. Genes & Development, 12, 3815–3820. doi: 10.1101/gad.12.24.3815.

Srivastava, A., MacKay, J. O., & Bell, J. B. (2002). A vestigial:scalloped TEA domain chimera rescues the wing phenotype of a scalloped mutation in Drosophila melanogaster. Genesis, 33, 40–47. doi: 10.1002/gene.10086.

Wu, S., Liu, Y., Zheng, Y., Dong, J., & Pan, D. (2008). The TEAD/TEF family protein scalloped mediates transcriptional output of the hippo growth-regulatory pathway. Developmental Cell, 14, 388–398. doi: 10.1016/j.devcel.2008.01.007.

Xiao, A., Cheng, Z., Kong, L., Zhu, Z., Lin, S., Gao, G., & Zhang, B. (2014). CasOT: A 234 genome-wide Cas9/gRNA off-target searching tool. Bioinformatics, 30, 1180–1182. doi: 10.1093/bioinformatics/btt764.

Ylla, G., Nakamura, T., Itoh, T., Kajitani, R., Toyoda, A., Tomonari, S., Bando, T., … Extavour, C. G. (2021). Insights into the genomic evolution of insects from cricket genomes. Communications Biology, 4, 733. doi: 10.1038/s42003-021-02197-9.

Zecca, M., & Struhl, G. (2007). Recruitment of cells into the Drosophila wing primordium by a feed-forward circuit of vestigial autoregulation. Development, 134, 3001–3010. doi: 10.1242/dev.006411.

Zecca, M., & Struhl, G. (2010). A feed-forward circuit linking wingless, fat-dachsous signaling, and the warts-hippo pathway to drosophila wing growth. PLoS Biology, 8, e1000386. doi: 10.1371/journal.pbio.1000386.

Zecca, M., & Struhl, G. (2021). A unified mechanism for the control of drosophila wing growth by the morphogens decapentaplegic and wingless. PLoS Biology, 19, e3001111. doi: 10.1371/journal.pbio.3001111.

Zhang, H., Shinmyo, Y., Mito, T., Miyawaki, K., Sarashina, I., Ohuchi, H., & Noji, S. (2005). Expression patterns of the homeotic genes Scr, Antp, Ubx, and abd-A during embryogenesis of the cricket Gryllus bimaculatus. Gene Expression Patterns, 5, 491–502. doi: 10.1016/j.modgep.2004.12.006.

Zhang, L., Ren, F., Zhang, Q., Chen, Y., Wang, B. & Jiang, J. (2008). The TEAD/TEF family of transcription factor scalloped mediates hippo signaling in organ size control. Developmental Cell, 14, 377–387. doi: 10.1016/j.devcel.2008.01.006.

FIGURE LEGENDS

Figure 1 Gene and amino acid structures of *sd* in *Gryllus bimaculatus*.

(a) Comparison of the Sd amino acid sequence between *Gryllus bimaculatus* (top) and *Drosophila melanogaster* (bottom). The *Gryllus sd* structure contained a conserved TEAD (amino acids 59–126) and YBD (amino acids 248–455). The *Drosophila sd* structure contains a TEAD (amino acids 62–130) and YBD (amino acids 198–407). The consistency rates of the domains were 99% for TEAD and 74% for YBD. (b) Gene structure of *Gryllus sd*. *sd* consisted of 11 exons and 10 introns within 300 kb. The gene structure was determined by Blast using *Gryllus sd* transcript data. The black arrow indicates the transcription start site.

Figure 2 Expression patterns of *Gryllus sd* during the embryo stage.

(a–h) Expression pattern of *sd* determined using *in situ* hybridization in stage 10 (a, b), 12 (c), and 16 (d–h) embryos. Enlarged view of stage 16 embryo legs (e), antennae (f), cerci (g), and dorsal segment (e), respectively. (a′–h′) Expression pattern of *sd* using the *sd*-eGFP line in stages 10 (a′, b′), 12 (c′), 16 (d′–h′), and 22 (i-o). Stages 10–16 (a′-h′) correspond to the results of *in situ* hybridization (a–h). Brightfield image (i). eGFP images of the head (k), dorsal segments (l), cerci (m), antenna and labrum (n), and T2 and T3 legs (o). The yellow signal is autofluorescence (j, l, n). Scale bars are 0.1 (a, c, d), and 0.5 mm (i).

Figure 3 Expression pattern of *sd* mRNA during the embryo stage.

(a–c) Negative control of *sd* staining in stages 10 (a), 12 (b), and 16 (c). (d–f) *sd* mRNA expression pattern in stages 10 (d), 12 (e), and 16 (f). Scale bars are 0.1 mm (a–f).

Figure 4 Generation of the *sd* enhancer trap line by knocking-in the eGFP expression vector.

(a) Schematic illustration of the GFP KI experiment. (b) G0 and G2 embryos of the *sd* enhancer trap strain. (c) Genotype experiment targeting the GFP-*sd* junction sequence. (d) Result of the GFP KI experiment. The enhancer trap method was based on that reported by Matsuoka et al. (2021) and Ohde et al. (2022).

Figure 5 Expression of *sd* in sixth-instar wing pads.

(a) Dorsal view of the sixth-instar wing pad before dissection. The wing pad was cut along the blue line. (b, c) Brightfield images of the dissected wing pad. Blue and orange lines correspond to the lines in panel (a). (d, e) eGFP images of the dissected wing pad. Red circles denote the eGFP-expressing area.

Figure 6 Expression dynamics of *Gryllus sd* in wing pads during the eighth instar and adult stages.

(a–r) Brightfield images of male (a–h) and female wing pads (j–q) and adult wings (i, r). (a′–r′) eGFP images of male (a′–i′) and female wing pads (j′–r′) and adult wings (i′, r′). Adult wings are white because of recent molting (i, i′, r, r′). Arrowheads denote eGFP signals in the proximal region (blue), trachea (yellow), bristles (pink), and margin area (orange). From day 1 to 6, wing pad tissue was observed on the cuticle because of fragility. From day 7 to adult, tissue was separated from the cuticle. White asterisks on red signals are autofluorescence by the residues of cuticles. Scale bar is 0.1 mm for (a-h), (a′–h′), and (i).

Figure 7 Summary of wing pad dissection.

The wing pads were cut along the blue line with dissecting scissors (a). The dorsal or ventral side of the cuticle was removed from the internal cell layer (b, c). The cell layer-attached side is presented for observation (d).

Fig. 6. Expression dynamics of *Gryllus sd* in wing pads during eighth instar and adult stages.

Figure 8 Comparison of *sd* expression patterns in eighth-instar wing pads between *sd* enhancer trap and in situ hybridization.

(a–d) An eighth-instar wing pad of the *sd* enhancer trap line. Overview (a), margin area (b), eGFP image of the bristle (c), and brightfield image of the bristle (d). (e–g) GFP staining as a positive control using the *sd* line. (h–j) Sense as the negative control of *sd* staining. (k–m) *sd* mRNA expression pattern. Blue circles indicate the margin area (c, d, g, j, m). Red circles indicate the bristle (b, f, i, l). In the control staining, the expression patterns in the basal hinge region and bristles were not clearly reflected, suggesting that the staining sensitivity is weak and potentially unreflective of all patterns. The proximal tissue was destroyed in the experimental process, and it could not be verified. In situ hybridization could only be performed in eighth-instar nymphs on day 5 (plus approximately 12 h).

Figure 9 Expression pattern of *sd* in the hindwings of eighth-instar nymphs.

(a–d) Brightfield images of the hindwing. (a′–d′ and e) eGFP images of the hindwing corresponding to the brightfield images. Lines indicate the proximal (blue) and distal

regions (red). The tissue of (d and d′) is flattened for observation. The spot fluorescence in (b′, c′, and e′) denotes bristles.

Figure 10 Identification of *sd*-expressing cells in wing bristles.

(a-c) Scanning electron microscopy image of the wing pad bristle. Overview (a). Cross-section view (b, c). (d–j) Confocal microscopy images of the wing pad bristle in the *sd* line. DAPI (d), eGFP (e), and merged images (f) on day 7. DAPI (g), anti-HRP antibody (h), eGFP (i), and merged images (j) on day 3. Red quotation marks denote the predicted location of the socket.

Figure 11 Effect of *Gryllus sd* KO during embryogenesis.

(a) Scheme of gRNA design. Red bars show the integration sites of gRNA. (b–e) Wild-type stage 22 embryo. Lateral view (b), ventral view (c), and head (d, e). Phenotypes of *sd* crispants (g–j). Lateral view (g), ventral view (h), and head (i, j). Blue arrows denote eyes (d, i) and antennae (e, j). (k) Wild-type first-instar nymph. (l–n) Phenotypes of *sd* crispants first-instar nymphs. (o) Table summarizing the outcome of *sd* crispants experiments.

Figure 12 Quantification of *sd* transcript expression following *sd* RNAi in third-instar nymphs.

(a) Transcript abundance in fourth-instar nymphs. (b) Transcript abundance in sixth-instar nymphs. (c) Transcript abundance in eighth-instar nymphs. Samples were obtained by cutting the T1–T3 thorax of three individuals and combining them into a

single sample. Relative expression was determined by the delta-delta Ct method. Results are the means of three experiments.

Figure 13 Effect of *Gryllus sd* nymphal RNAi.

(a) Schematic illustration of the *sd* dsRNA design. Two dsRNAs were designed, with both producing the same phenotype. (b–g) *DsRed* control and phenotypes of *sd* RNAi. Adults injected with 3 μg of DsRed as the control (b, c). Adults injected with 3 μg of dsRNA in the seventh instar (d, e). Adults injected with 3 μg of dsRNA in the third instar (f, g). Arrowheads denote antennae (blue), legs (pink), cerci (green), and ovipositors (orange). The result of nymphal RNAi is presented in Table 2. Scale bar is 0.5 mm for (b–g).

Figure 14 Analysis of the wing phenotype following *Gryllus sd* RNAi.

(a–d) Dorsal view of eighth-instar nymphs and adults injected with a high concentration of dsRNA for *sd* RNAi in the third instar. DsRed as a negative control (a, b), eighth instar (c), and adult (d). (e–g, e′–g′) Effect of low-concentration *sd* RNAi. Wild-type (e, e′), adults injected with 0.03 μg of dsRNA in the seventh instar (f, f′), and adults injected with 0.03 μg of dsRNA in the third instar (g, g′). (f–h) Illustration of the wing area compared to *sd* RNAi phenotypes. Wild-type (gray), phenotype following injection in the seventh instar (blue), and phenotype following injection in the third instar (pink). (j) Wing area ratio of wild-type vs. *sd* RNAi in the third instar. This landmark method is based on Klingenberg et al. (2010). Blue bar denotes wild-type, and the orange bar denotes *sd* RNAi. (k) Measurement of proliferating cells in the margin area by EdU incorporation

experiments. Blue bar denotes DAPI-positive cells, and the green bar denotes EdU-positive cells.

Figure 15 Effect of *sd* RNAi on male wings and determination of the wing area.

(a) Wild-type adult wing. The proximal (Pr), distal (D), anterior (A), and posterior (Po) axes are indicated. (b) The wing of an adult subjected to *sd* RNAi in the seventh instar. (c) The wing of an adult subjected to *sd* RNAi in the third instar. (d) Determination of the area of the wing was performed as described previously (Bennet-Clark et al., 2002; Montealegre-Z et al., 2011). (g) Location of spots used in the landmark (red circle). Landmark analysis was performed as described previously (Klingenberg et al., 2010). The scale bar is 0.5 mm for (a–c).

Figure 16 Comparison of wing morphology between wild-type adults and adults subjected to *sd* RNAi in the third instar.

Comparison of the wing area determined by landmark analysis (as described in Figure S9) between wild-type adults and those subjected to *sd* RNAi in the third instar. Data are presented as the mean ± SD (n = 5). *p < 0.05; **p < 0.005; Student's t-test.Measuring of proliferation cells by EdU experiment

Figure 17 Measurement of proliferating cells by EdU incorporation experiments.

(a) A wild-type wing pad treated with EdU on day 3 in the eighth instar. (b) Wing pad subjected to *sd* RNAi and treated with EdU on day 3 in the eighth instar. Blue squares show the margin area where proliferating cells were counted. (c, d) GFP and DAPI

staining of the margin area (100 μm2) in wild-type adults and adults subjected to *sd* RNAi. The thick linear green signal is tracheal autofluorescence.

Figure 18 *Gryllus* and *Drosophila sd* expression during wing development

In *Drosophila*, the dorsal-ventral (DV) boundaries are determined in second-instar larvae, and *sd* is ubiquitously expressed throughout the pouch region of the wing disc. By contrast, in *Gryllus*, *sd* is expressed in the margin area at least in the sixth-instar, and its expression rapidly increases from the mid to late stages. Thereafter, expression decreases rapidly during molting and rebounds as the stage progresses. This expression contributes to the continuous growth of the wing pad margin area and shows a more localized pattern than that in *Drosophila.*

Figures

Fig. 1

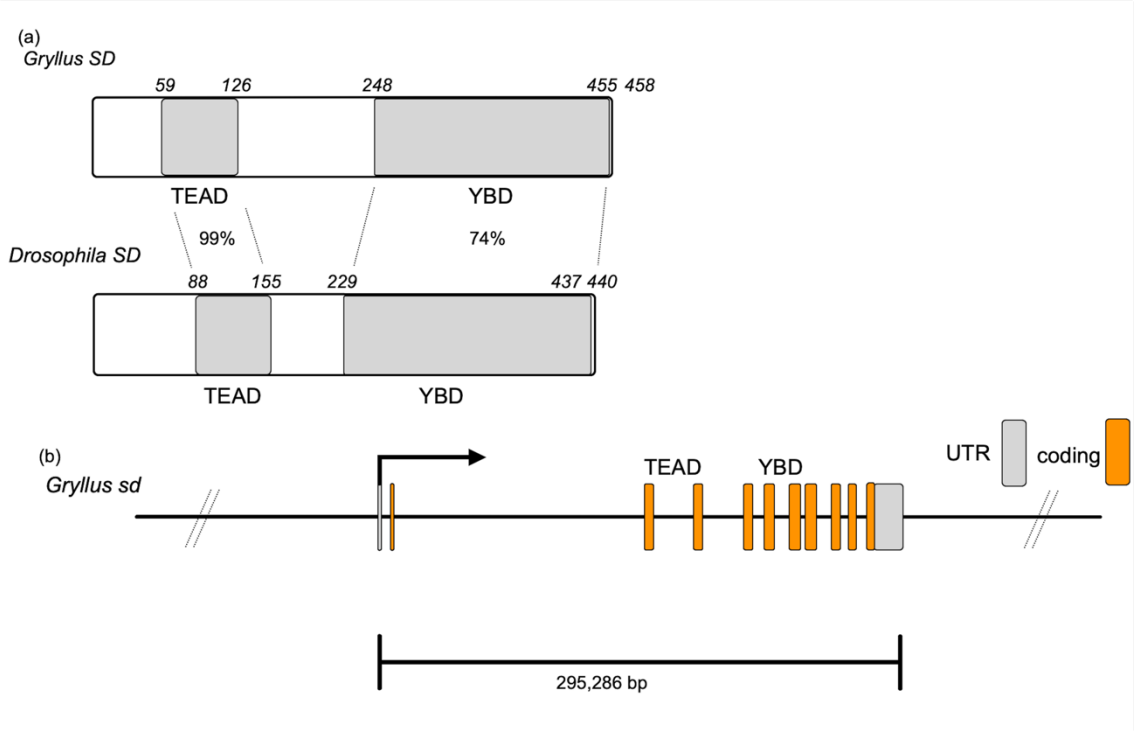

Fig. 2

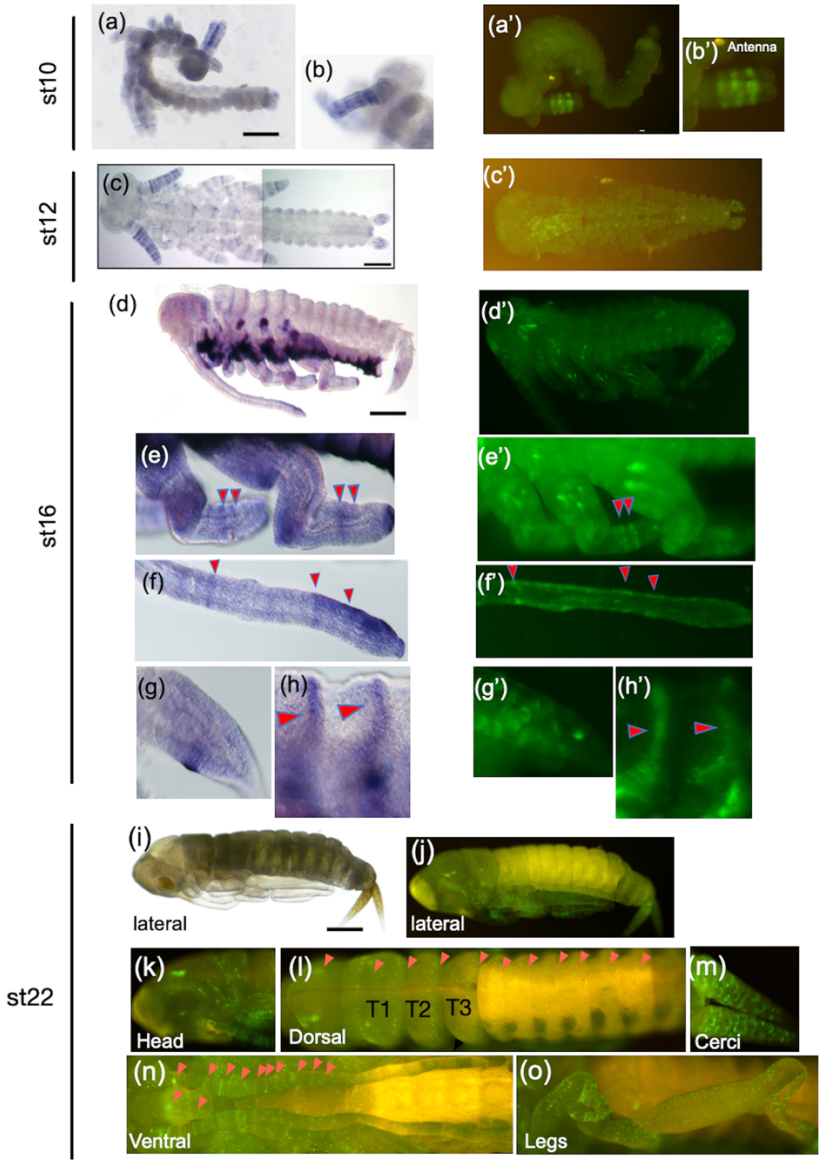
st10
st12
st16
st22
(a)
(b)
(a')
(b') Antenna
(c)
(c')
(d)
(d')
(e)
(e')
(f)
(f')
(g)
(h)
(g')
(h')
(i)
lateral
(j)
lateral
(k)
Head
(l)
T1 T2 T3
Dorsal
(m)
Cerci
(n)
Ventral
(o)
Legs

Fig. 3

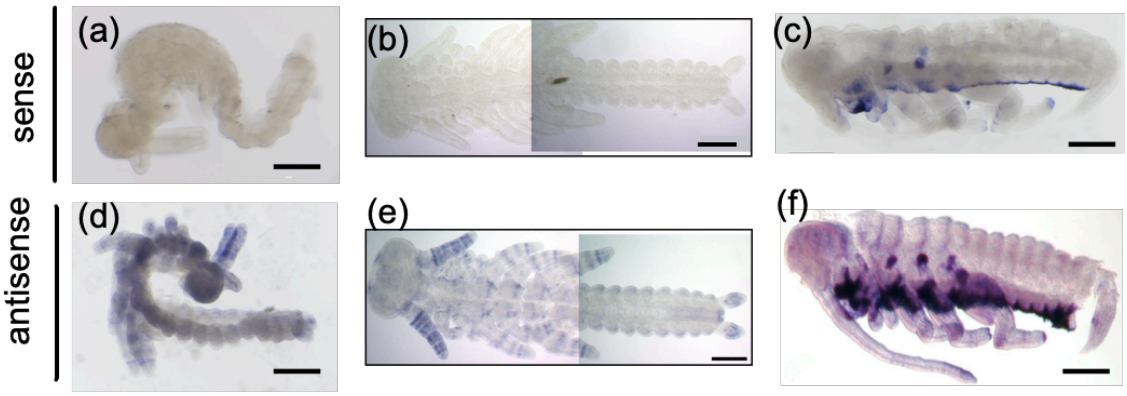

Fig. 4

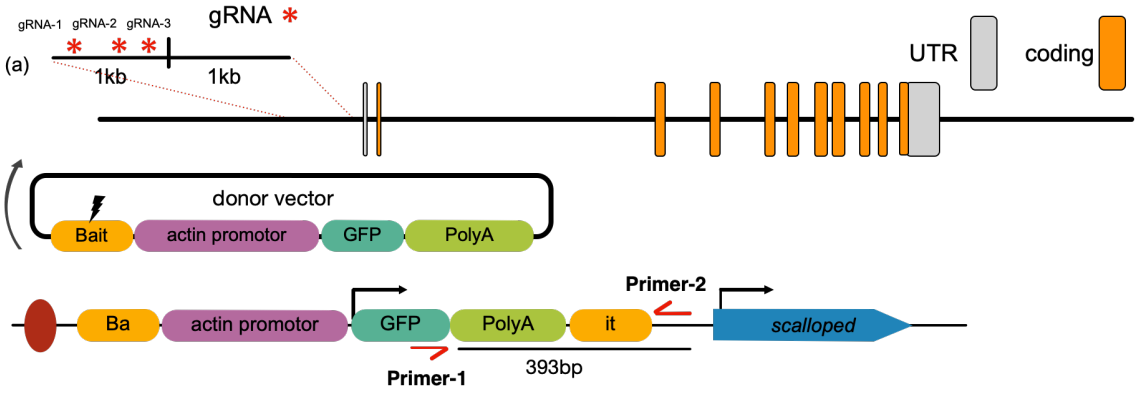

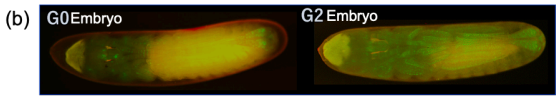

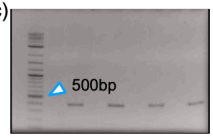

eGFP-*sd* junction region 393bp

(d)

gRNA	No. of injected eggs	Developed	GFP positive	Germline transmission
gRNA-1	58	39(68%)	0(0%)	0(0%)
gRNA-2	58	19(32%)	1(1%)	0(0%)
gRNA-3	95	65(68%)	3(3%)	1(1%)

Fig. 5

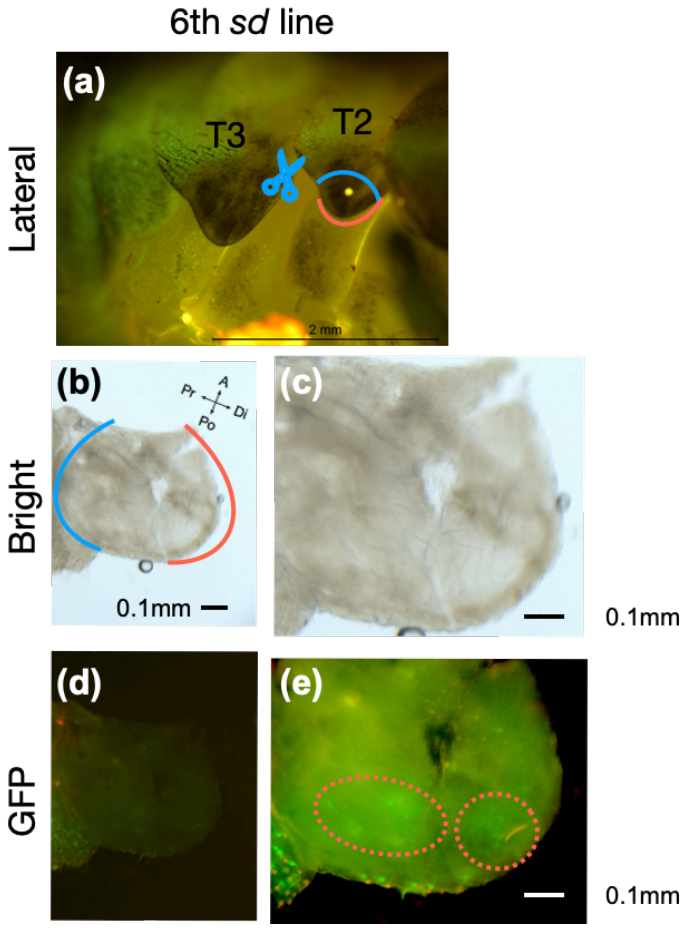
6th sd line
Lateral
Bright
GFP
(a)
T3
T2
2 mm
(b)
Pr
A
Di
Po
0.1mm
(c)
0.1mm
(d)
(e)
0.1mm

Fig. 6

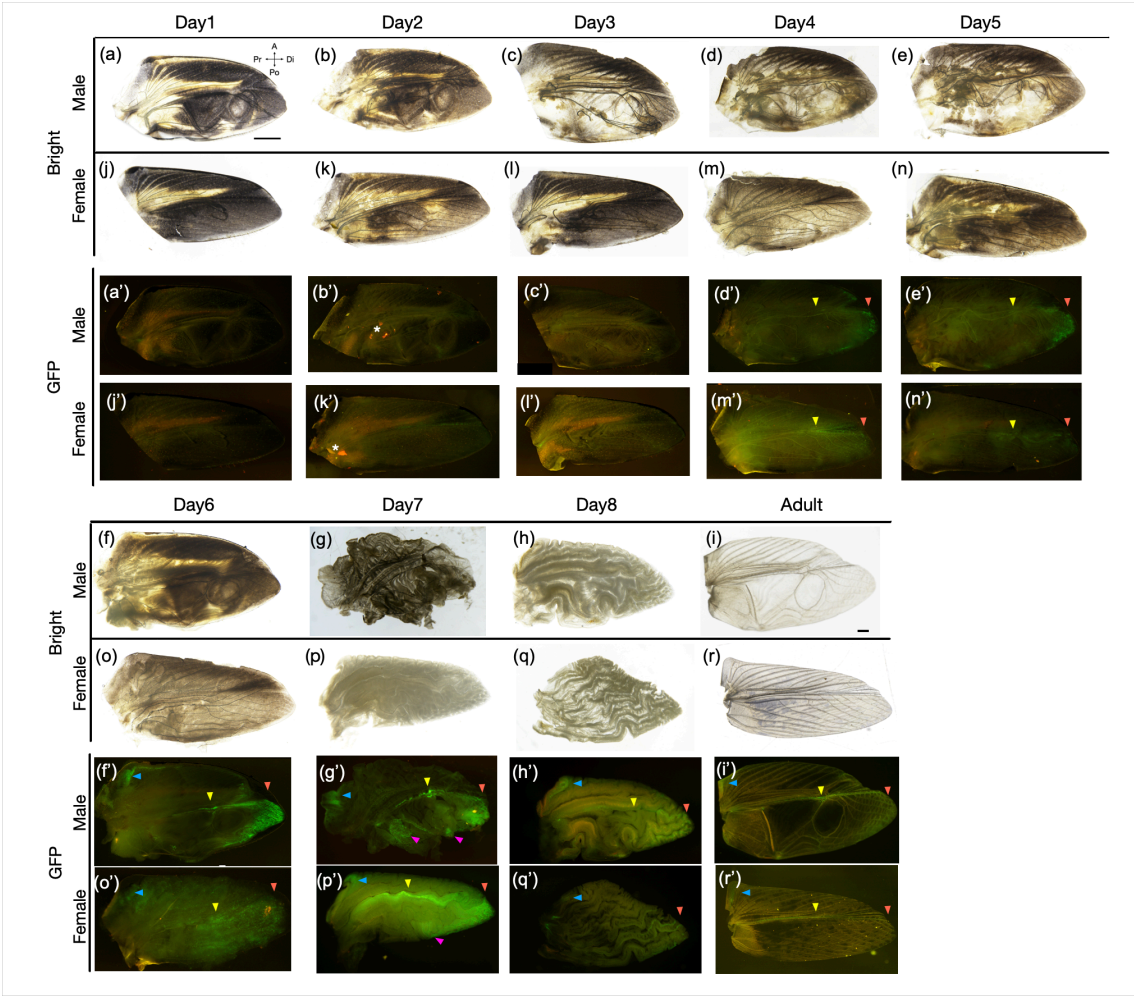
Day1
Day2
Day3
Day4
Day5
Bright
Male
Female
GFP
Male
Female
(a)
(b)
(c)
(d)
(e)
(j)
(k)
(l)
(m)
(n)
(a')
(b')
(c')
(d')
(e')
(j')
(k')
(l')
(m')
(n')
Day6
Day7
Day8
Adult
Bright
Male
Female
GFP
Male
Female
(f)
(g)
(h)
(i)
(o)
(p)
(q)
(r)
(f')
(g')
(h')
(i')
(o')
(p')
(q')
(r')

Fig. 7

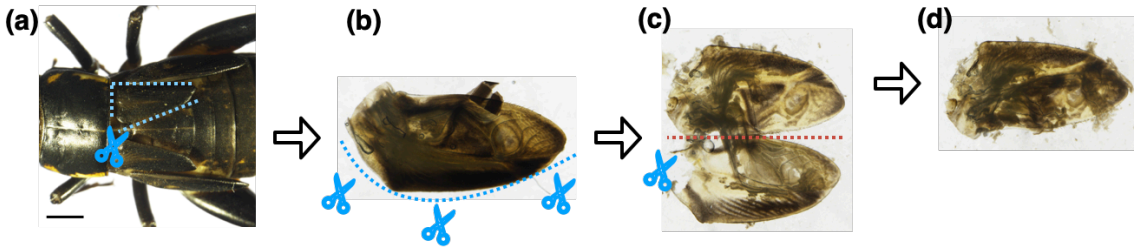

Fig. 8

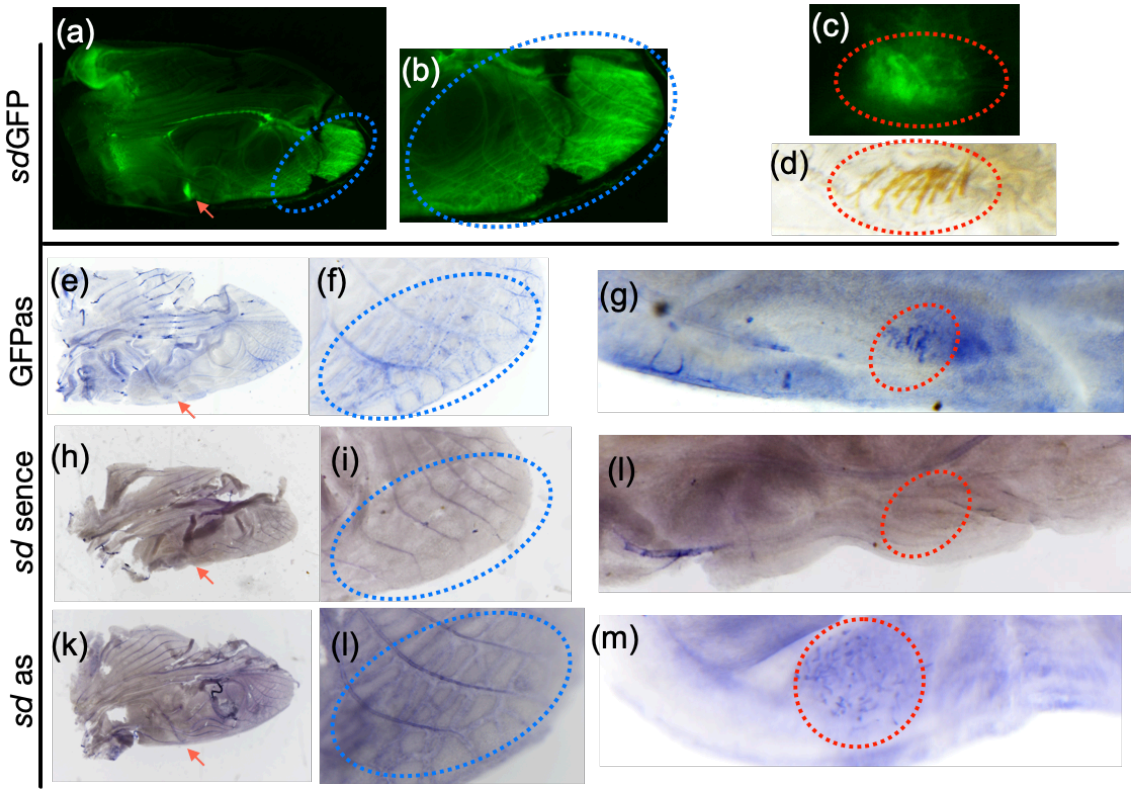

Fig. 9

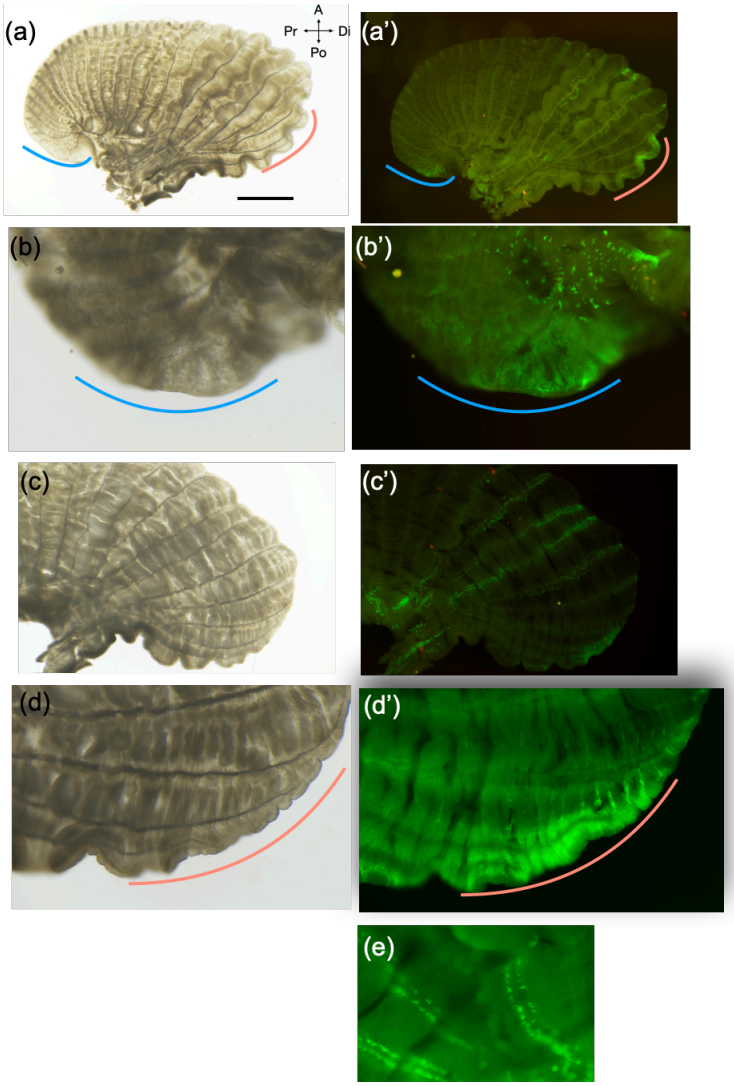

Fig. 10

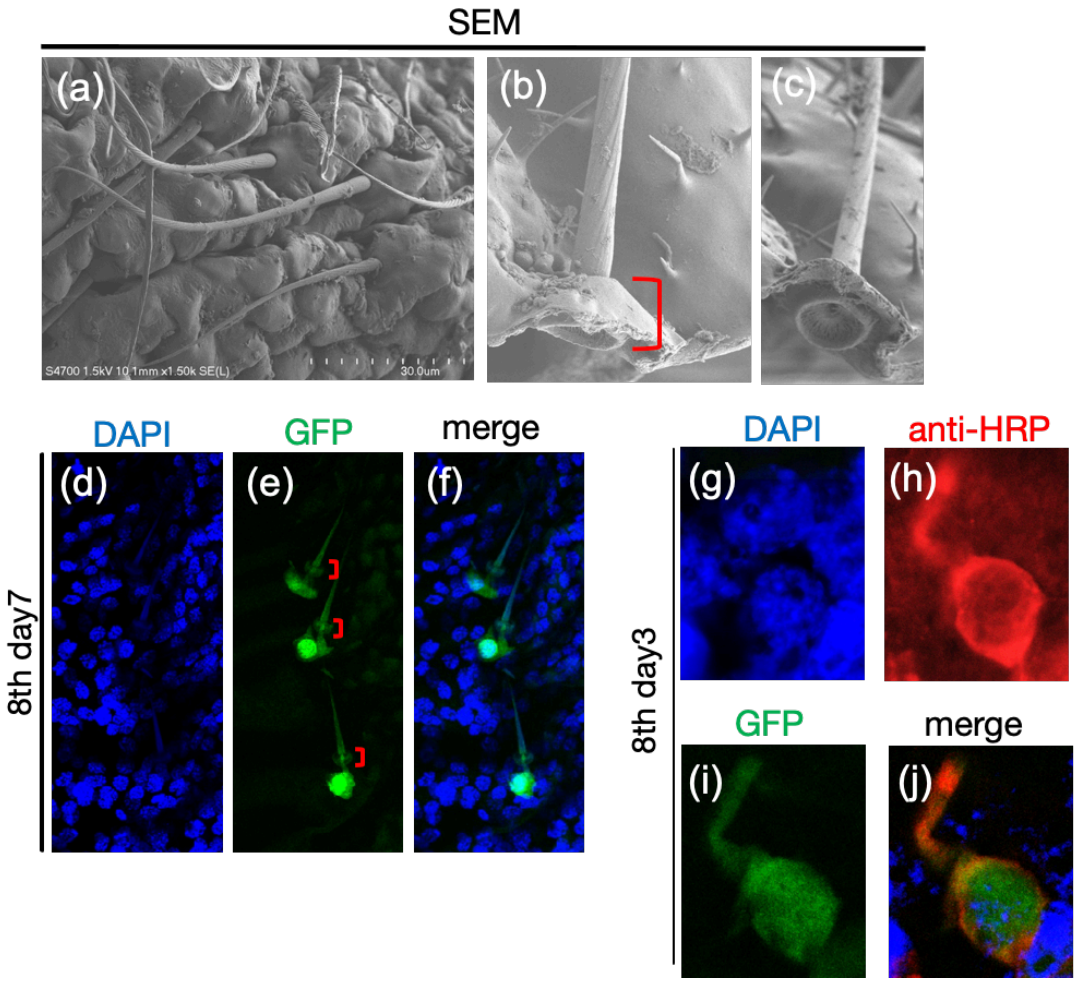
SEM
(a)
(b)
(c)
S4700 1.5kV 10.1mm x1.50k SE(L)
30.0um
DAPI
GFP
merge
8th day7
(d)
(e)
(f)
DAPI
anti-HRP
8th day3
(g)
(h)
GFP
merge
(i)
(j)

Fig. 11

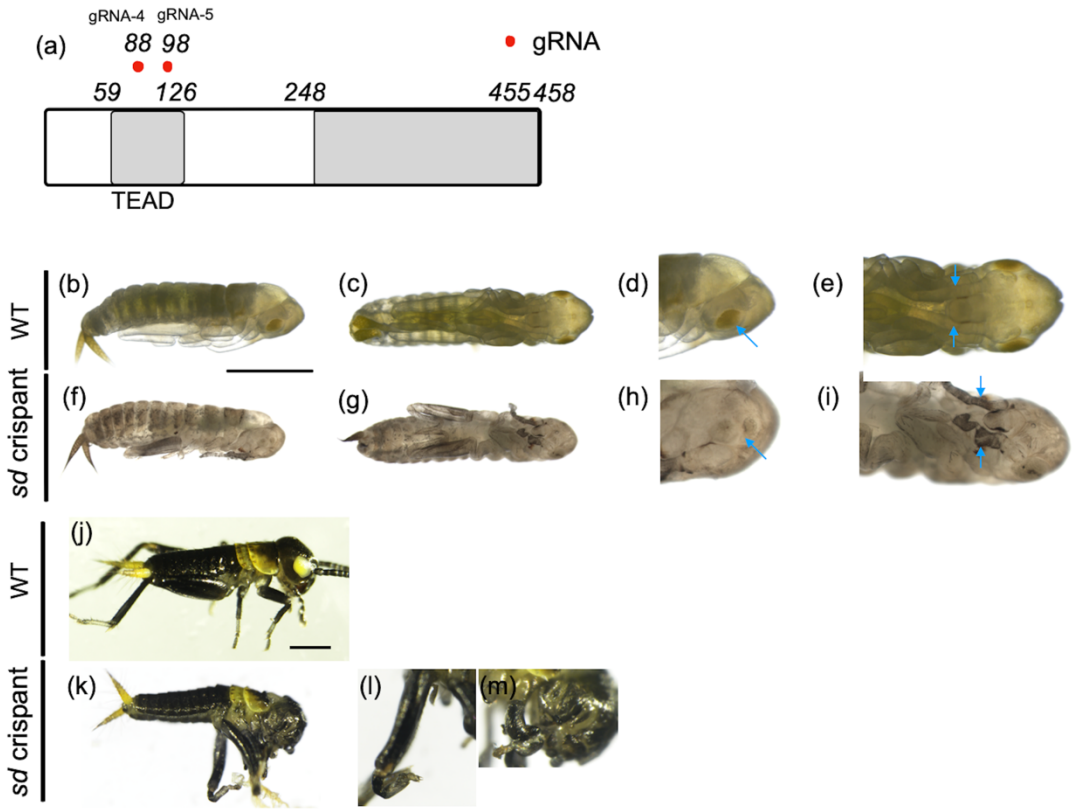

(n)

	Injected nymphs	Lethal at st1-st15	Lethal at st15-st24	Hatched
NO injection	60	4(8%)	0(0%)	52(92%)
GFP	60	9(15%)	0(0%)	51(85%)
sd crispants	500	434(87%)	56(11%)	10(2%)
Parental RNAi	100	100(100%)	0(0%)	0(0%)

Fig. 12

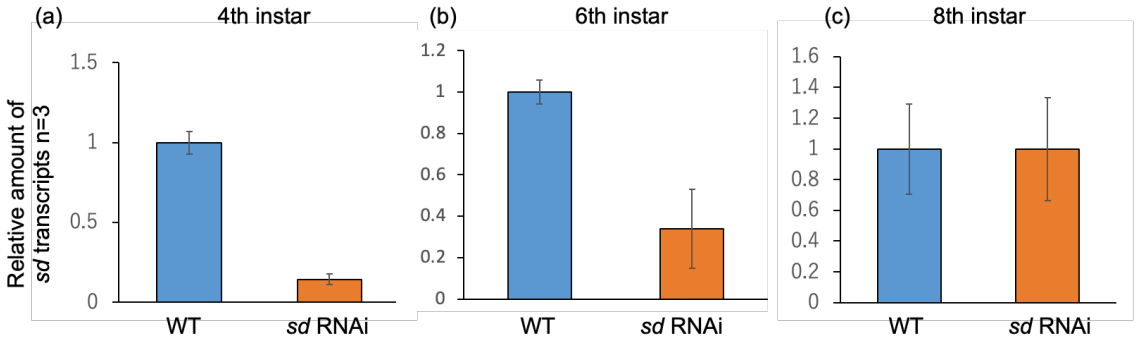
(a)
4th instar
(b)
6th instar
(c)
8th instar
Relative amount of sd transcripts n=3
1.5
1
0.5
0
1.2
0.8
0.6
0.4
0.2
1.6
1.4
WT
sd RNAi

Fig. 13

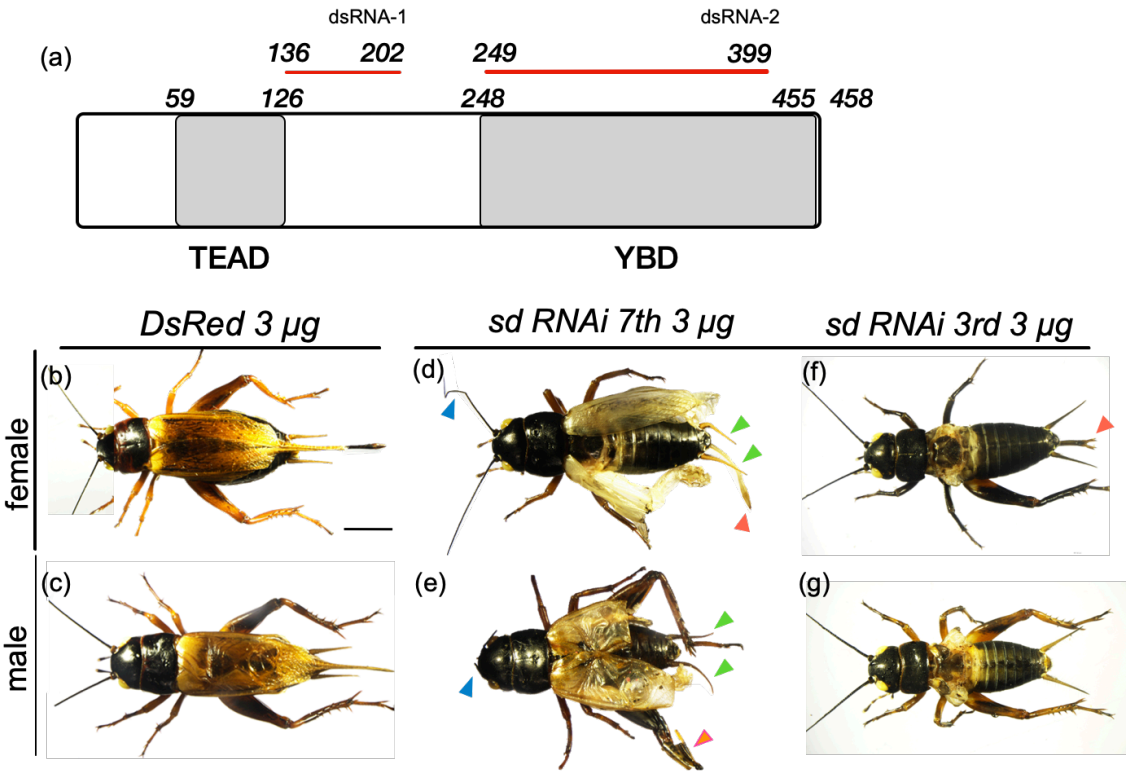
(a)
dsRNA-1
dsRNA-2
136
202
249
399
59
126
248
455
458
TEAD
YBD
DsRed 3 μg
sd RNAi 7th 3 μg
sd RNAi 3rd 3 μg
female
male
(b)
(c)
(d)
(e)
(f)
(g)

Fig. 14

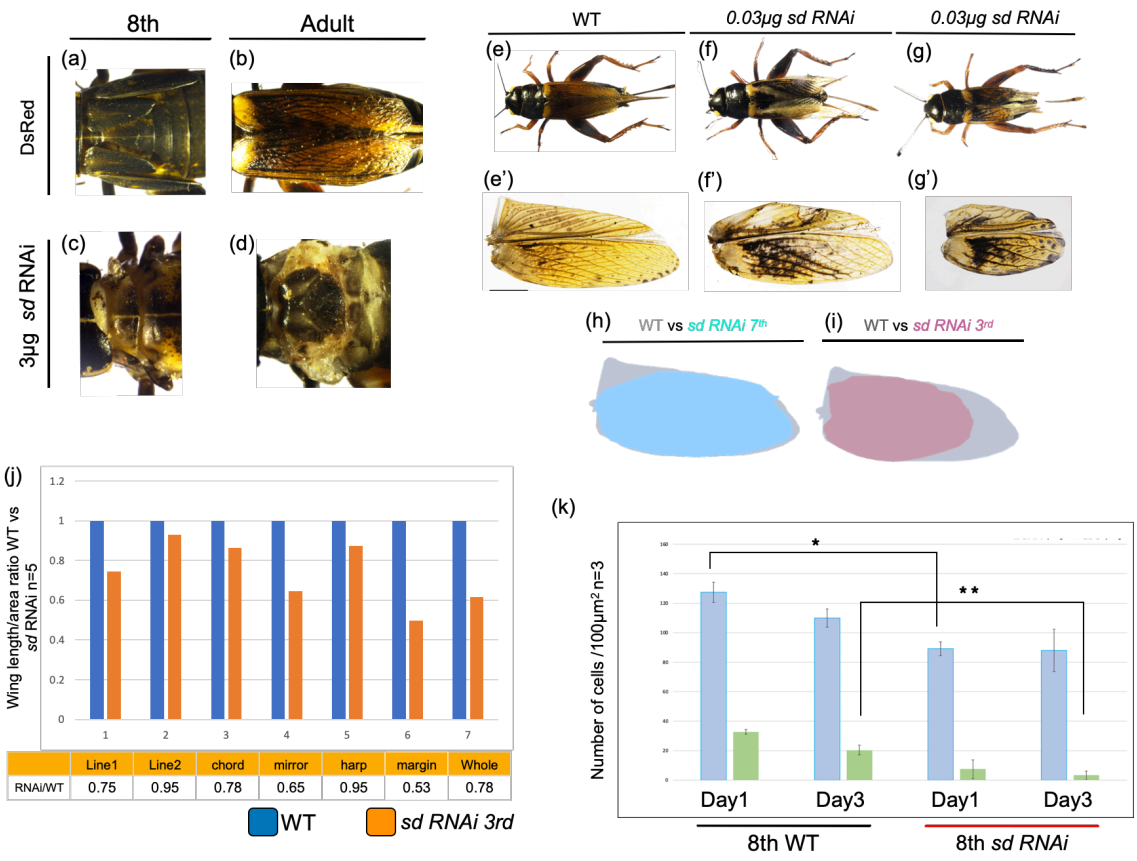
8th
Adult
(a)
(b)
DsRed
3μg sd RNAi
(c)
(d)
WT
0.03μg sd RNAi
0.03μg sd RNAi
(e)
(f)
(g)
(e')
(f')
(g')
(h) WT vs sd RNAi 7th
(i) WT vs sd RNAi 3rd
(j)
Wing length/area ratio WT vs sd RNAi n=5
1.2
1
0.8
0.6
0.4
0.2
0
1
2
3
4
5
6
7
Line1 Line2 chord mirror harp margin Whole
RNAi/WT 0.75 0.95 0.78 0.65 0.95 0.53 0.78
WT
sd RNAi 3rd
(k)
Number of cells /100μm² n=3
*
**
Day1
Day3
Day1
Day3
8th WT
8th sd RNAi

Fig. 15

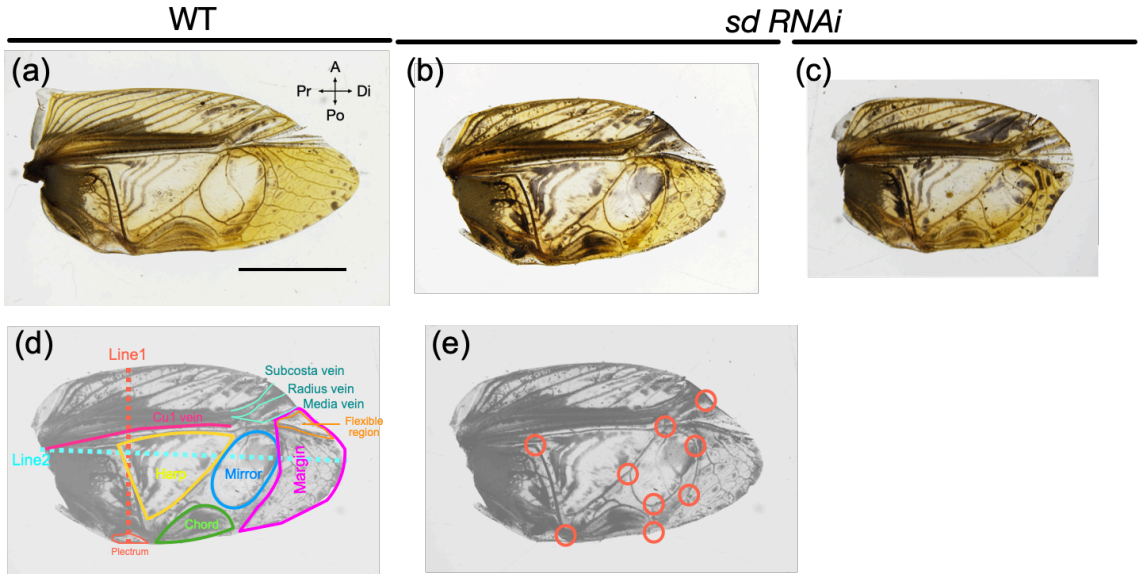
WT
sd RNAi
(a)
A
Pr
Di
Po
(b)
(c)
(d)
Line1
Subcosta vein
Radius vein
Media vein
Flexible region
Line2
Hamp
Mirror
Margin
Chord
Plectrum
(e)

Fig. 16

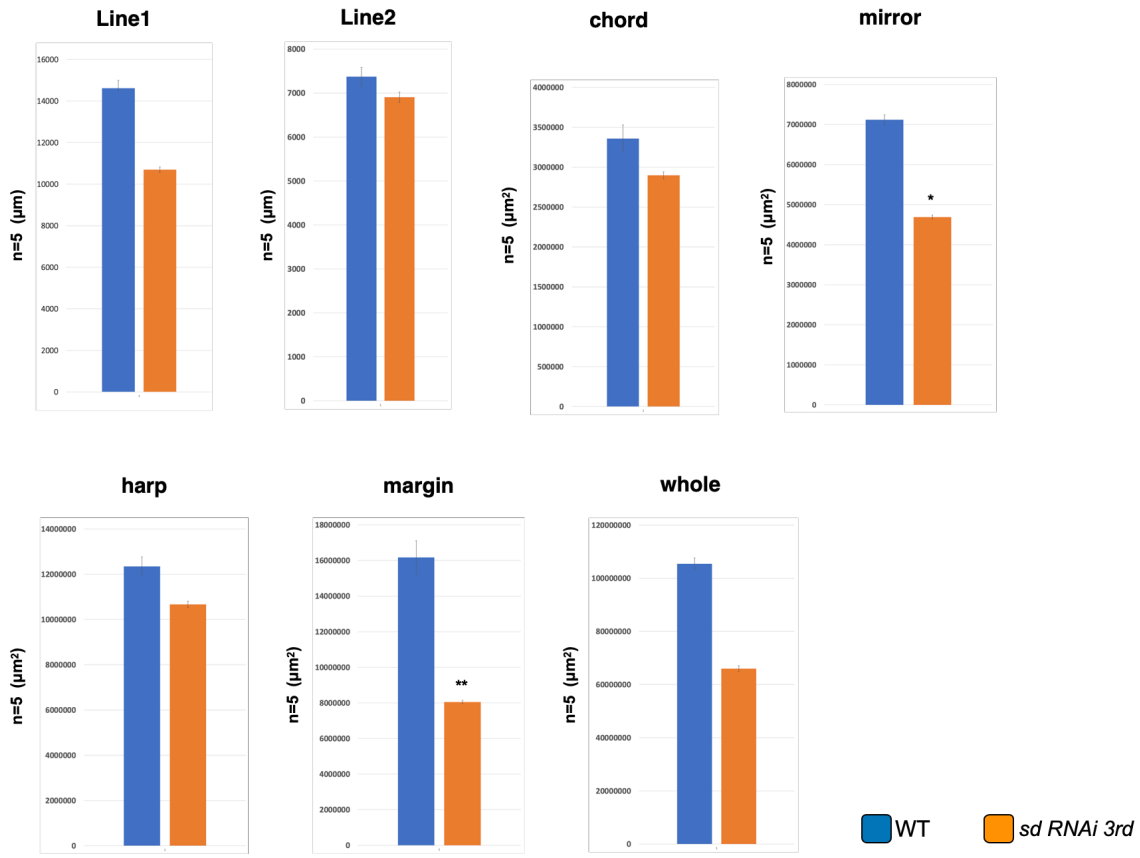
Line1
Line2
chord
mirror
harp
margin
whole
n=5 (μm)
n=5 (μm²)
*
**
WT
sd RNAi 3rd

Fig. 17

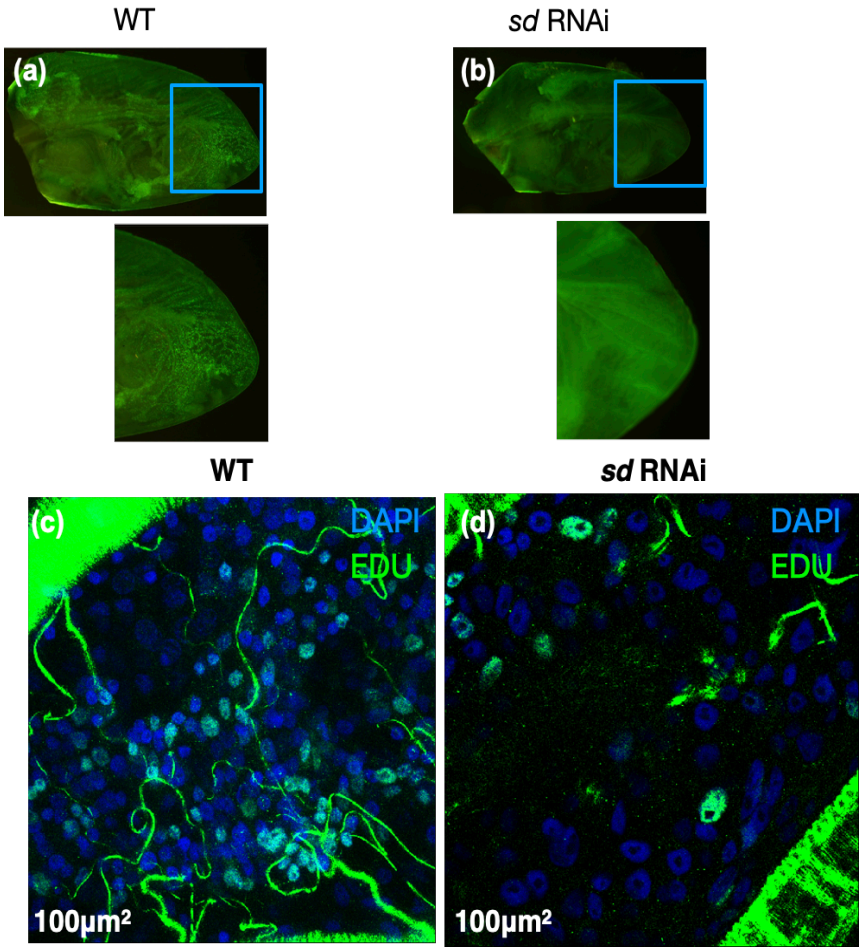

Fig.18

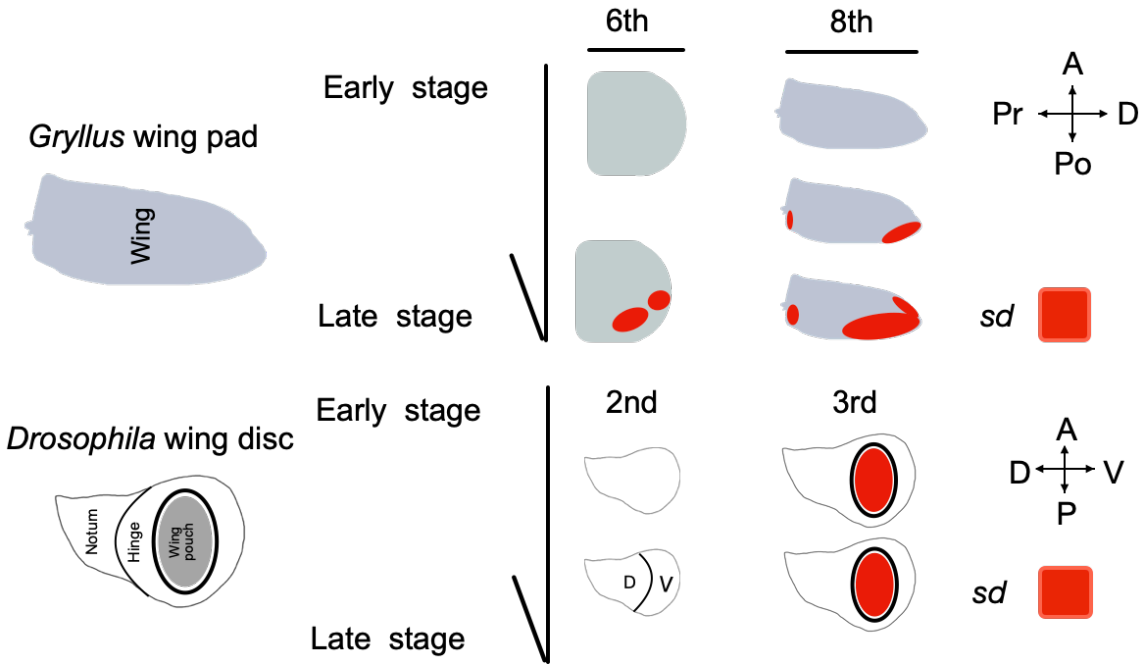
6th
8th
Early stage
Gryllus wing pad
Wing
A
Pr
D
Po
Late stage
sd
Early stage
2nd
3rd
Drosophila wing disc
Notum
Hinge
Wing pouch
A
D
V
P
D
V
Late stage
sd

Table 1 Sequences of gRNAs and PCR primers used in this study

gRNA sequence for GFP knock-in	
gRNA-1	GTACTGTCAGAGGACAACTA
gRNA-2	GTGAGACGAGTTACTCTCCGG
gRNA-3 (Line-generated)	GATATTAATGAGCGCTCGCG
gRNA sequence for *sd* knock-out	
gRNA-4	CCGCCGCAAGATCATCCTGT
gRNA-5	GCAGAGCTTCCAGGAGGCGC
Primers for *sd* junction PCR	
Primer-1 (*sd* genome)	ACCTTTGTATGTTCCATTCGAGAGA
Primer-2 (GFP)	CGAGTTCATGCGCTTCAAGGT
Primers for qPCR	
qPCR-1 (*sd*)	CCAGGTGTTGGCTAGAAGGAAAT
qPCR-2 (*sd*)	CTATCTGTGCACTTGACATGCTG
qPCR-3 (*β-actin* as reference)	AAAACTGCCCTGGGTGCAT
qPCR-4 (*β-actin* as reference)	TTGACAATGGATCCGGAATGT
Primers for *sd* cDNA cloning	
Primer-3	TCGGGAGCGGTAGATGTACGAGTT
Primer-4	TCCATTATGCGTTGCACTCACCCA
Primers for dsRNA template liniar DNA	
Primer-5 (sd_T7 Fw[1])	GTAATACGACTCACTATAGGGCCCAGGTGTTGGCTAGAAGGA
Primer-6 (sd_T7 Rv[1])	GTAATACGACTCACTATAGGGCCCTGGGTAGGACACTGGAGA
Primer-7 (sd_T7 Fw[2])	GTAATACGACTCACTATAGGGCTGTGGAGTTCTCTGCCTTTATGGAA
Primer-8 (sd_T7 Rv[2])	GTAATACGACTCACTATAGGGCACGTGATGGTCATGTTTTCATTGCT
Primers for ish probe template liniar DNA	
Primer-9 GFP (antisense)	ACGTAAACGGCCACAAGTTC
Primer-10 T7_GFP (antisense)	GTAATACGACTCACTATAGGGTGCTCAGGTAGTGGTTGTCG
Primer-11 GFP(sense)	TGCTCAGGTAGTGGTTGTCG
Primer-12 T7_GFP(sense)	GTAATACGACTCACTATAGGGACGTAAACGGCCACAAGTTC
Primer-13 sd (antisense)	TCAGCTACAGCTATCCACAACAA
Primer-14 sd_T7 (antisense)	TAATACGACTCACTATAGGGAAGGAAGAAAGCATTTTGAGGTC
Primer-15 sd (sense)	AAGGAAGAAAGCATTTTGAGGTC
Primer-16 sd_T7 (sense)	TAATACGACTCACTATAGGGTCAGCTACAGCTATCCACAACAA

***Primer sets are distinguished by color**

Table 2 The results of *sd* nymphal RNAi

RNAi at 3rd nymph	No of injected	No of survival at adult	No of phenotype at adult / survival
DsRed	21	15(71%)	0(0%)
sd 198bp	19	8(42%)	8(100%)
sd 450bp	22	15(68%)	13(81%)
RNAi at 7th nymph	No of injected	No of survival at adult	No of phenotype at adult / survival
DsRed	16	15(71%)	0(0%)
sd 198bp	16	16(100%)	8(50%)
sd 450bp	16	15(94%)	7(47%)